Modeling of gas dynamic behaviour of CCSO in nanostructured media

Andrey A. Markov[*], Igor A. Filimonov[**] and Karen S. Martirosyan[***]

[*]Institute for Problems in Mechanics of the Russian Academy of Sciences,
101 Vernadskogo ave, B1, Moscow, 119526, Russia
[**]Institute of Structural Macrokinetics and Material Science of the Russian Academy of Sciences,
Chernogolovka, Moscow Region, Chernogolovka, 142432, Russia
[***]University of Texas at Brownsville, Department of Physics and Astronomy,
80 Fort Brown, Brownsville, TX, 78520, USA

ABSTRACT

Recently a novel, simple and energy efficient synthesis of nanoparticles of complex oxides referred to as Carbon Combustion Synthesis of Oxides, (CCSO) was developed. In CCSO the exothermic oxidation of nanoscale carbon generates a thermal reaction wave with relatively low temperatures that propagates through the solid reactant mixture converting it to the desired oxide products. The carbon used in the CCSO is not incorporated in the product and is emitted from the sample as a CO_2. The high rate of CO2 release helps to form a highly porous (up to 0.7) and friable product, having a particle size in range 50-800 nm. This phenomenon results from a vortex gas flow in the reaction zone fed by the carbon dioxide co-flow and oxygen counter-flow filtration. It is characterized by alternate (stratified) macroscopic regions of large particles and low gas pressure. In contrast to the classical problems of filtration combustion it deals with the Navie-Stokes equation rather than with the Darcy law or Euler equation on the macroscopic level. This is a more general description which in combination with a non-uniform and self-organizing porosity of the combusting sample leads numerically first to a weak spin instability of the CCSO front and then to fingering at the latest combustion stages.

Keywords: carbon combustion synthesis, modeling of gas dynamic, nanostructured media, multi-phase flow

1. INTRODUCTION

Nanotechnology have experienced phenomenal growth and recent fundamental, applied and experimental developments have notably contributed to progress and have motivated further developments and enhancements. Nanostructured complex oxides have unique novel properties different from those of bulk materials and they are becoming a core component of advanced materials that have many practical applications. Their rapid growing market demand calls for cost-effective and environmentally friendly technologies for large-scale production. Recently, Martirosyan and Luss [1, 2] invented a new, simple, economical and energy efficient synthesis of submicron and nanostructured complex oxides from inexpensive reactant mixtures. In this process, referred to as Carbon Combustion Synthesis of Oxides (CCSO) [3, 4], where the exothermic oxidation of carbon

$$C^{(s)} + O_2^{(g)} = CO_2^{(g)} \quad \Delta H^{298}_{CO_2} = -393.5 \text{ kJ/mol}$$

generates a self-sustained thermal reaction wave with temperature gradient of up to 1000 °C/cm that propagates at a velocity of 0.1-3 mm/s through the solid reactant mixture (oxides, carbonates or nitrates) converting it to the desired oxide product by the reaction:

$$\sum_{i=1}^{n} \mu_i X_i^{(s)} + \alpha C^{(s)} + \beta O_2{}^{(g)} = \sum_{j=1}^{m} P_j^{(s)} + \delta CO_2{}^{(g)} + (-\Delta H) \qquad (1)$$

where $X_i^{(s)}$ is a solid compound, i.e. an oxide, super oxide, nitride, or carbonate, chloride, or oxalate) containing the metal needed to form the oxide, $P_j^{(s)}$ the solid complex oxide product, μ_i, β and δ stoichiometric coefficients and (-ΔH) the heat of the reaction and $\alpha = \dfrac{x/12}{(100-x)/\sum \mu_i M_i^{(s)}}$, where x is the carbon weight percent in the mixture and $M_i^{(s)}$ the molecular weight of the *i-th* reactant. The goal of this study was to determine gas dynamic behaviour of CCSO producing $BaTiO_3$ by the reaction:

$$BaCO_3 + TiO_2 + \alpha(C+O_2) = BaTiO_3 + (\alpha+1)CO_2{}^{\uparrow}.$$

The micro and macro scale technique for strongly coupled two-phase flows proposed by Markov [5, 6] is applied to simulate thermal front propagation in porous media.

2. COUNTER GAS FLOW AND FILTRATION COMBUSTION

The mechanism of complex oxide formation by CCSO is rather complex, as it is influenced by the several simultaneous physical and chemical processes such as carbon heating, oxygen infiltration and decomposition of some reactants, formation of CO, CO_2 and oxygen counter flow, and solid-solid reactions between oxides [7]. Thus, the CCSO consists of several reaction steps the first being

carbon combustion. Figure 1 shows schematic of the CCSO. It well known that carbon oxidation proceeds by the reactions:

$$C(s)+1/2O_2(g)\rightarrow CO(g)\ \Delta H=-110.5\ kJ/mol;$$
$$C(s)+O_2(g)\rightarrow CO_2(g)\ \Delta H=-394.5\ kJ/mol.$$

The CO may be oxidized as it diffuses to the sample surface by the reaction $CO(g)+1/2O_2(g)\rightarrow CO_2(g)$ $\Delta H=-283.1$ kJ/mol. The equilibrium level of carbon monoxide depends on the temperature and oxygen concentration. Increasing the oxygen concentration and temperature in the reaction zone decreases the CO concentration [8]. Gas-spectroscopy analysis of the CCSO gaseous products did not detect any carbon monoxide, indicating that if any carbon monoxide was formed in the initial stage of the reaction it was converted to CO_2 [4]. Some of the present carbonate or oxides, such as $BaCO_3$ and TiO_2, probably may have catalyzes the CO oxidation to CO_2. The highly exothermic carbon oxidation increased the local temperature leading to a temperature front propagation, decomposition of $BaCO_3$ and rapid formation of product by solid state reaction between the simple oxides: $BaO+TiO_2\rightarrow BaTiO_3$. The heat needed for these endothermic (20 kJ/mol) reactions is provided by the carbon combustion.

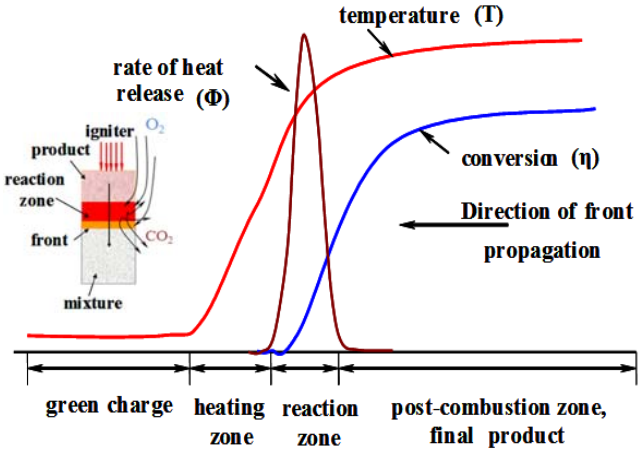

Figure 1: Schematic of the CCSO: Carbon is not incorporated into the product and emit from sample.

In the CCSO there is oxygen consumption in the CCSO preheated layer and carbon dioxide release in the post combustion zone. Thus, the gas dynamic structure of the CCSO isn't simple but rather complex. Two opposite countercurrent flows of oxygen and carbon dioxide take place inside the reaction zone. They penetrate each other or create vortexes dependent on the reactive mixture porosity and the concentration or/and temperature disbalance between the sample inlet and outlet. As vortex sources we may imagine the co-flow filtration of carbon dioxide and counter flow filtration of oxygen. In spite of the fact that the vortex possibility certainly exist, one need always keep in mind that these countercurrent gaseous flows are week enough and don't even influence directly the CCSO temperature. The mechanism of heat transfer during the CCSO is rather thermal conductivity than gas convection.

3. FORMULATION OF THE MICROSCOPIC PROBLEM

Let us consider an arbitrary set of L simultaneous chemical reactions involving K distinct chemical species. The bulk and surface reactions are written as follows:

$$\sum_{j=1}^{K}\eta_{ij}^{'}C_j \underset{k_{ir}^{vol},-Q_i^{vol}}{\overset{k_{if}^{vol},Q_i^{vol}}{\rightleftarrows}} \sum_{j=1}^{K}\eta_{ij}^{''}C_j,$$
$$\sum_{j=1}^{K}\nu_{ji}^{'}C_j \underset{k_{ir}^{S},-Q_i^{S}}{\overset{k_{if}^{S},Q_i^{S}}{\rightleftarrows}} \sum_{j=1}^{K}\nu_{ji}^{''}C_j, \qquad i=1,...,L \qquad (2)$$

Here $\eta_{ij}^{'},\eta_{ij}^{''}$ and $\nu_{ij}^{'},\nu_{ij}^{''}$ are appropriate stoichiometric coefficients for j th' specie in the i'th chemical process for bulk and surface reaction respectively. The values $k_{if}^{vol},k_{ir}^{vol}$ are the reaction rate constants for forward and backward bulk reactions and Q_i^{vol} denote their thermal effect. All the reaction rates included in the CCSO are thermally activated and the corresponding temperature dependence has been taken in account in the model by their reaction rate constants. The values k_{if}^{S},k_{ir}^{S} and Q_i^{S} are the rate constants and thermal effects for surface reactions. Let components C_l, $l=1,...,K_p$; $K_p<K$ change the phase from gas to solid due to chemical condensation $C_l \xrightarrow[Q_l^{ph}]{k_l^{ph}} P_l$. Including the phase transition, the mass rate production $\dot{M}_j^{S}$ specie C_j for an arbitrary set of L simultaneous surface reaction steps is presented in Ref. 5. Let C_j and M_j are the mass fraction and molar mass of j^{th} specie, ρ is gas density, J_j^{ph} is the condensation rate of specie, $\dot{M}_j^{vol}$ is the mass flux for bulk reaction, $c_{j,b}^{sat}$ is concentration of saturated vapor of intermediate product C_j over particle surface of radius b, the value of $J_j^{ph}=k_j^{ph}\left(\frac{C_{jS}\rho_S}{M_j}-c_{j,b}^{sat}\right)$, $j=1,....,K_p$; $J_j^{ph}=0$, $j>K_p$

Using the balance equations of mass and energy, we write down the micro-level equations for a spherical condensed particle of volume V_b and surface square $S_b=4\pi b^2$ in a gas volume V as follows [5]:

$$\frac{1}{S_b}\frac{\partial\left(\rho_S C_{jS}V\right)}{\partial t}=\dot{M}_j^{S}-M_j J_j^{ph}+\beta_j(C_{j,ex}-C_{jS})\rho_S \qquad (3)$$

where β_j are the microscopic mass transfer coefficients

$$\frac{1}{S_b}\frac{\partial C_b \rho_p V_b T_S}{\partial t} = \dot{Q}_S + k\left(T_{ex} - T_S\right) \qquad (4)$$

$$\frac{1}{S_b}\frac{\partial \rho_p V_b}{\partial t} = \left(1 - \frac{V_b}{V}\right)\sum_{j=1}^{n_p} M_j J_j^{ph} \qquad (5)$$

$\dot{Q}_S$ is the thermal source due to surface reaction, $k-$ is the microscopic heat transfer coefficient, C_b is specific heat of particle at constant pressure, ρ_p is particle density. The subscripts ex and S are referred to values near (at some distance: $r = r_{ex} > b_0 \equiv b\big|_{t=0}$ from the particle center) and at the particle surface correspondingly. The saturated concentration $c_{j,b}^{sat}$ with respect to j specie depends on critical radius $b_{j,cr}$ of a condensed particle and on saturated vapor concentration at plane surface $c_{j,\infty}^{sat}$. These values are found using thermodynamics consideration. The heat transfer and mass transfer coefficients k and β_j depend on the coordinates of a particle. These values are found resolving the flow problem near the particle in the region $b(t) < r < r_{ex}$ [6].

$$\frac{D\rho C_j}{Dt} - \dot{M}_j^{vol} = \nabla_r \cdot \left(\rho D_j \nabla_r C_j\right) \qquad (6)$$

$$\frac{D\rho C_p T}{Dt} - \dot{Q}^{vol} = \nabla_r \cdot \left(\lambda \nabla_r T\right) \qquad (7)$$

$r = b(t)$: $\quad C_j = C_{jS};\ T = T_S$;

$r = r_{ex}$: $C_j = C_{j,ex};\ T = T_{ex}$. As the result of solution, we come to the microscopic coefficients:

$$\beta_j = \frac{D_{jS}}{\left(C_{j,ex} - C_{jS}\right)}\frac{\partial C_j}{\partial r}\bigg|_S,\ j = 1,...,n;$$

$$k = \frac{\lambda_S}{\left(T_{ex} - T_S\right)}\frac{\partial T}{\partial r}\bigg|_S \qquad (8)$$

$\beta_j -$ is the microscopic mass transfer coefficient, D_j is diffusivity. $k-$ is the microscopic heat diffusivity. We use the notion for any given functions φ and ψ:

$$\nabla_r \cdot \left(\psi \nabla_r \varphi\right) \equiv \frac{1}{r^2}\frac{\partial}{\partial r}\left(\psi r^2 \frac{\partial \varphi}{\partial r}\right); \quad \frac{D\varphi}{Dt} \equiv \frac{\partial \varphi}{\partial t} + \frac{u_P}{r^2}\frac{\partial \varphi r^2}{\partial r} \qquad (9)$$

where u_P is the local velocity. The microscopic problem is formulated for each individual particle in local spherical coordinates. After the appropriate averaging procedure the macro fluxes are calculated and macro scale equations are solved in cylindrical coordinates.

4. NUMERICAL SCHEME AND COMPUTATION RESULTS

The self-consistent numerical solution of microscopic equations into each cell and macroscopic equations is applied using the splitting technique [5]. The equations are solved numerically using implicit finite difference approximations. Consider a computational cell which volume is $V(x,y,z)$ and the center is located at a node (x,y,z). Let $V(x,y,z)\,n(x,y,z)$ be the number of particles uniformly distributed inside the cell and $b(x,y,z)$ be the radius of particles. At the first step the heat and mass microscopic transfer coefficients and the values on the particle surface are found by solving the system of equations (3-7). At the second step the averaged surface mass and thermal fluxes J_l^{het}, J_j^{ph} are calculated for macro scale resolution. The results of computation refer to particle number density: $n_0 = 5\cdot 10^{12}$, $z_{kb} = 5\cdot 10^2$, $b_0 = 10^{-6}$. The reference temperature is $T_0^{'} = 1000K$ and the ignition takes place at the right side (outlet) $X = 1$ of the tube (cylindrical sample). Reynolds and Peclet numbers are equal to 10^3 and thermal Peclet number was varied from 10^{-4} to 10. We considered the combustion kinetics described by Eq. (2) as follows: $L = 1, K = 3, K_p = 1; \nu_{11}^{''} = 1,\ \nu_{12}^{''} = 0,\ \nu_{13}^{''} = 0,\ \nu_{11}^{'} = 0,\ \nu_{12}^{'} = 2,\ \nu_{13}^{'} = 0$ These are the simplest examples of previously studied kinetics [7] with minimum parameters which help us to determine the influence of initial and boundary conditions on flow patterns when condensation takes place. It turns out that the reaction kinetics already studied and their combinations partially represent by themselves the model of CCSO reaction kinetics. The dimensionless parameters of computation are k_1^0, k_2^0, Q_0, Q_s, Q_{ph}. We assume below that $k_{1r}^{vol} = k_{1r}^{S} = 0$, $k_{1f}^{vol} = k_{1f}^{S} = k_1^0$, $k_1^{ph} = k_2^0$, $Q_1^{vol} = Q_0$, $Q_1^{S} = Q_s$, $Q_1^{ph} = Q_{ph}$. The rate parameters used are: $k_1^0 = 10^9$, $k_2^0 = 10^6$. Regular computations were performed on grid 51 and 41 nodes in axial and radial direction respectively and the number of time steps was about several thousands.

Figure 1 shows the simulation of wave motion and particle size distribution. The calculation shows that the higher initial right-hand temperatures and the higher temperature disbalance under other equal conditions may lead to formation of local macroscopically large regions with large-size particles along the sample core (about 1.7 times larger than those near the walls and inlet). These regions are localized near the sample central axis: at the distance of a half of the sample radius from the wall and about the 1/4 of the radius from the outlet. Evidently that

formation of the macroscopically large region containing a sufficient number of large-size particles causes consumption of vast oxygen and therefore leads to formation of macroscopically large evacuated regions (of low gas density) inside the CCSO sample.

Figure 2 shows distribution of gas velocity during the CCSO. The calculation revealed that the complicated finger front instability can be developed. This phenomenon results from a vortex gas flow in the reaction zone fed by the carbon dioxide co-flow and oxygen counter-flow filtration.

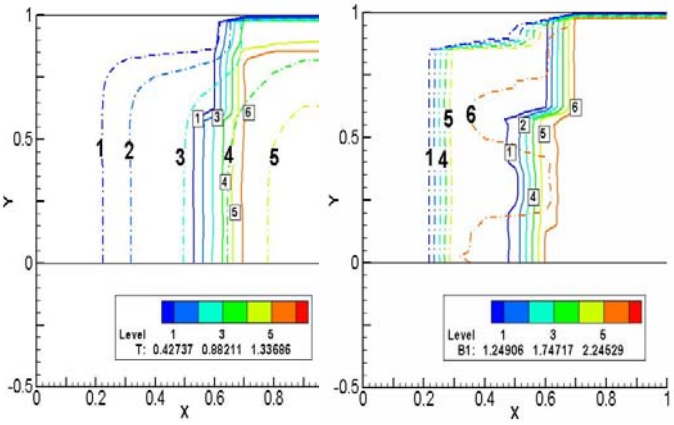

Figure 2: (left) The temperature field distribution $T(t^n, x)$ in time. (right) The particle size distribution $b_1(t^n, x)$ in time. Solid lines and dots correspond to time level $n = 100$ and $n = 2500$, respectively. The results are presented for thermal effect of reactions as follows $Q_0 = 49,\ Q_s = 400,\ Q_{ph} = 1.5$. The rate parameters are $k_1^0 = 10^9,\quad k_2^0 = 10^6$.

Figure 2 shows the formation of fingers instability patterns at different initial parameters. The patterns are sharper and more ramified at low pressure and become smoother and more circular at high pressure. The finger instability developed during CCSO is accompanied by complex gas dynamics. According to general physical concept the higher thermal Peclet numbers generates more stable plane combustion motion. this means that the more plane-closed combustion front motion is actually formed.

The gas dynamic behaviour of CCSO is a typical example of highly nonlinear multiple scale problem. It is characterized by alternate (stratified) macroscopic regions of large particles and low gas pressure. In contrast to the classical problems of filtration combustion it deals with the Navie-Stokes equation rather than with the Darcy law or Euler equation on the macroscopic level. This is a more general description which in combination with a non-uniform and self-organizing porosity of the combusting sample leads numerically first to a weak spin instability of the CCSO front and then to fingering at the latest combustion stages. The numerical results obtained are in a qualitative agreement with the experimentally observed microscopic pictures.

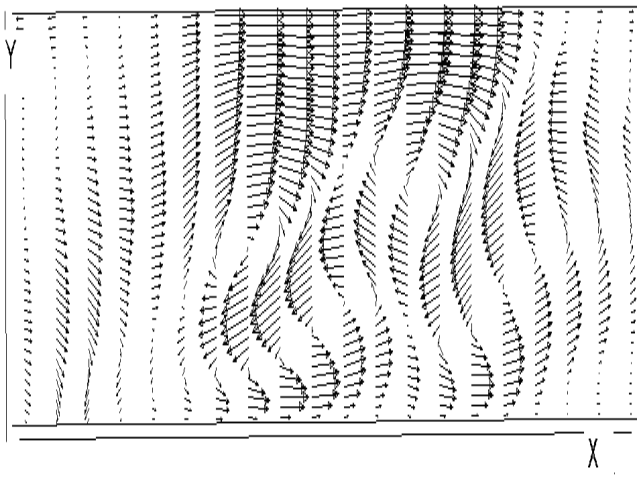

Figure 3: Computed distribution of gas velocity during CCSO.

ACKNOWLEDGMENTS

We would like to acknowledge the financial support of this research by the National Science Foundation, grant 0933140.

REFERENCES

[1] K.S. Martirosyan and D. Luss, AIChE J., 51, 10, 2801-2810, 2005.

[2] K.S. Martirosyan and D. Luss, Ind. Eng. Chem. Res., 46, 1492-1499, 2007.

[3] K.S. Martirosyan and D. Luss, Chem. Eng. Technology, 32, 9, 1376-1383, 2009.

[4] K.S. Martirosyan and D. Luss, US Patent 7,897,135, March 1, 2011. .

[5] A.A. Markov, CFD Journal, 16, 3, 28, 268-281. 2008.

[6] A.A. Markov, Computational Fluid Dynamics, Proceedings of the Fourth International Conference on Computational Fluid Dynamics, 753-758, 2009.

[7] A. Markov, I. Filimonov and K.S. Martirosyan, Thermal Reaction Wave Simulation using Micro and Macro Scale Interaction Model, pp. 929-936, in book, Computational Fluid Dynamics 2010, ed. by A. Kuzmin, Springer, p. 995, 2011.

[8] L.D Smoot, and P.J. Smith, Coal Combustion and Gasification; Plenum Press: New York – London, p. 443, 1985.

[9] A.A. Markov and I.A. Filimonov, Theoretical Foundations of Chemical Engineering, 42, 5, 477–485, 2008.